Unraveling Molecular Flexibility in Prebiotic Chemistry: Tiopronin under the Lens of Rotational Spectroscopy and Quantum Chemistry

Lina Uribe,[†,‡] Sergio Mato,[¶] Luigi Crisci,[‡] Sofia Municio,[¶] Elena R. Alonso,[¶] José L. Alonso,[¶] Iker León,[*,¶] and Vincenzo Barone[*,§]

†*Scuola Normale Superiore di Pisa, Piazza dei Cavalieri 7, 56126 Pisa, Italy*

‡*Scuola Superiore Meridionale, Largo San Marcellino 10, 80138 Napoli, Italy*

¶*Grupo de Espectrocopía Molecular (GEM), Edificio Quifima, Laboratorios de Espectroscopia y Bioespectroscopia, Unidad Asociada CSIC, Parque Científico UVa, Universidad de Valladolid, 47011 Valladolid, Spain*

§*INSTM, via G. Giusti 9, 50121 Firenze, Italy*

E-mail: iker.leon@uva.es; vincebarone52@gmail.com

Abstract

Tiopronin, an N-substituted glycine derivative bearing a thiol group, offers a compelling structural analogy to HS-peptides—molecules of growing interest in prebiotic chemistry. These thiol-terminated peptides, potentially formed through abiotic dry-down reactions of mercaptoacids and amino acids, represent a plausible alternative to classical peptide formation under early Earth conditions. In this work, we investigate the conformational landscape of tiopronin by combining high-resolution microwave spectroscopy with state-of-the-art quantum-chemical calculations. Using an unsupervised computational framework that integrates multiple methods while balancing accuracy and efficiency, we predict the low-energy conformers detectable in microwave experiments and compute their ground-state rotational constants. An unbiased validation of the resulting conformational landscape is obtained through direct comparison with experiment, enabled by the accuracy attained in the computed spectral parameters. This integrated approach not only provides detailed structural insight into tiopronin but also contributes to a broader understanding of molecular complexity emerging from prebiotic chemical pathways. Moreover, the generality of the proposed framework makes it well suited for the structural characterization of other thiolated amino acids and peptide-like systems of prebiotic and biochemical relevance.

1 Introduction

Tiopronin is an N-substituted derivative of glycine that can be formally viewed as the product of a condensation reaction between thiolactic acid and glycine (see Figure 1). Specifically, the carboxylic acid group of thiolactic acid reacts with the amino group of glycine, forming an amide bond. This linkage is structurally and chemically analogous to the peptide bonds that connect amino acids in peptides and proteins.[1] Amide bonds play a fundamental role in nature, as they constitute the backbone of protein structures and enable the formation of complex biological macromolecules from simple amino acid units.

The biological significance of proteins has motivated extensive efforts to understand their chemical origins, particularly within the context of prebiotic chemistry. A central objective in this field is to identify plausible pathways for peptide formation under primitive Earth conditions, predating enzymatic catalysis and cellular machinery.[2] However, it is well known that the abiotic condensation of amino acids into peptides faces both thermodynamic and kinetic constraints, including high activation barriers and the necessity of water removal—conditions not easily met in early Earth environments.[2]

Recent studies have proposed alternative mechanisms to overcome these barriers. In particular, dry-down reactions between mercaptoacids and amino acids can yield HS-peptides, in which the typical N-terminal amine is replaced by a thiol group.[3] Although these species feature the same amide linkage as conventional peptides, they exhibit distinct reactivity and stability. Tiopronin serves as a modern analogue of such systems: its terminal thiol group makes it a valuable model for exploring prebiotic peptide formation and its structural consequences.

Structurally, tiopronin also presents significant conformational flexibility due to multiple rotatable bonds and polar functional groups. Accurately characterizing its conformational landscape requires both sensitive spectroscopic techniques and robust computational models.

Rotational spectroscopy in the microwave (MW) region is one of the most powerful

tools for such studies. Since rotational constants are directly related to the molecular geometry and atomic masses, and different conformers generally have distinct moments of inertia, MW spectroscopy provides an unambiguous means to identify and differentiate conformers, isomers, and isotopologues. In recent years, the technique has been successfully applied to thermolabile solids—such as many molecular bricks of life—thanks to the development of laser ablation (LA) sources.[4–9] The subsequent supersonic-jet expansion cools the molecules to very low rotational temperatures, greatly simplifying the spectra. Additionally, chirp-pulse MW spectrometers,[10,11] combined with fast-mixing nozzles, have enabled the characterization of large molecular systems and non-covalent interactions.[12–15] MW spectra of simple dipeptides and analogues have thus been interpreted with the aid of DFT calculations.[16,17] Nevertheless, only high-level quantum chemical methods can provide the accuracy required for predictive MW spectra without resorting to chemical intuition or external data.[18] Composite post-Hartree–Fock approaches have been successfully employed for the glycine dipeptide analogue,[7] but their application to larger and more flexible systems is limited by prohibitive computational cost and the need to explore multiple low-energy conformers. Moreover, achieving spectroscopic accuracy demands vibrational corrections that depend on semi-diagonal cubic force constants, which are themselves expensive to compute.

Based on these premises, we have developed and validated in the last two years the family of Pisa composite schemes (PCS),[19,20] which combines the efficiency of lower-level methods with the accuracy of high-level ab initio calculations through a systematic strategy. Furthermore, fast numerical procedures for the computation of diagonal and semi-diagonal third energy derivatives have been implemented.[21]

Leveraging these tools, we investigate the potential energy surface of tiopronin, identify its low-energy conformers, and compute their equilibrium and vibrationally corrected rotational constants. These predictions allow direct comparison with experimental MW spectra and enable reliable conformational assignments. Our work exemplifies how the synergy between high-resolution microwave spectroscopy and state-of-the-art quantum chemical modeling can

yield detailed structural insights into biologically and prebiotically relevant molecules such as tiopronin.

2 Methods

2.1 Experimental details

A commercial sample of tiopronin (TCI, 97%) was used without further purification. A solid cylindrical rod was prepared by mixing the sample with a small amount of commercial binder (Peoval 33). The resulting mixture was pressed, inserted into the ablation nozzle, and vaporized using the third harmonic (355 nm) of a picosecond Nd:YAG laser (20 mJ per pulse, 20 ps pulse width). The vaporized species were then supersonically expanded with neon as the carrier gas at a backing pressure of 10 atm.

The resulting molecular jet was analyzed using a Chirped Pulse Fourier Transform Microwave (CP-FTMW) spectrometer coupled to the laser ablation (LA) system.[22–24] Spectra were recorded in the 6–12 GHz region. A pulsed valve, synchronized at 2 Hz, was used to generate the supersonic expansion into the vacuum chamber of the spectrometer, ensuring rotational cooling of the molecules.

The microwave excitation pulse was generated by a 24 GS s^{-1} arbitrary waveform generator (AWG), which produced a 4 μs chirped pulse in the 3–6 GHz range. This signal was frequency-doubled and amplified by a 300 W traveling wave tube amplifier (TWTA) to induce a macroscopic polarization in the sample. The resulting free induction decay (FID) signals were detected in the time domain using a 50 GS s^{-1} oscilloscope. Up to 80,000 individual FID signals were recorded, with four FIDs collected per valve cycle. These were averaged and subsequently Fourier transformed to obtain the final frequency-domain spectra.

2.2 Computational details

Different variants of the Pisa Composite Schemes (PCSs),[19] characterized by increasing levels of accuracy, are employed in a general exploration/exploitation strategy refined and validated in several recent studies.[25–28] The main steps of the workflow are as follows:

1. Initial identification of a broad panel of low-energy minima through conformational sampling using three different force fields (OPLS2005, MMFFs, and Amber). Torsional/low-mode sampling was performed with an energy window of 35 kJ/mol, employing the Maestro suite from the Schrödinger program.[29]

2. Geometry optimization and analysis of relaxation pathways between adjacent minima using the B3LYP functional with the 6-31+G* basis set and D3BJ dispersion corrections. This computational model is referred to as HPCS2.

3. Evaluation of accurate geometries and harmonic force fields for the most stable minima not involved in rapid relaxation via the rev-DSD-PBEP86-D3BJ double-hybrid functional[30] and the 3F12$^-$ basis set.[31] The latter is derived from the standard cc-pVTZ-F12 basis set[32] by removing d functions on first-row atoms and replacing the two f functions on second- and third-row atoms with a single one from the cc-pVTZ set.[33] This computational model is referred to as DPCS3.

4. Further refinement of equilibrium geometries by applying one-parameter corrections to DPCS3 bond lengths (referred to as BDPCS3).[34] These corrections, Δr^{BCV} and Δr^{BV}, are applied only to bond distances:

$$r^{BDPCS3} = r^{rDSD/3F12-} + \Delta r^{BCV} + \Delta r^{BV} \tag{1}$$

where

$$\Delta r_{ij}^{BCV} = K_{n_i,n_j} \tag{2}$$

and

$$\Delta r_{ij}^{BV} = K'_{n_i,n_j} r^{rDSD/3F12-} \tag{3}$$

with n_i and n_j being the atomic numbers of the bonded atoms. The K and K' coefficients are related to the covalent radii and Pauling bond orders, respectively.[34,35] Notably, BDPCS3 results can be obtained at the same cost as a standard DFT optimization.

5. Computation of spectroscopic parameters and relative populations under experimental conditions, using BDPCS3 geometries. Since MW spectroscopy yields ground-state rotational constants, vibrational corrections must be included. These are incorporated via:

$$B_\tau^0 = B_\tau^{eq} + \Delta B_\tau^{vib} \tag{4}$$

where B_τ^{eq} and ΔB_τ^{vib} denote the equilibrium constant and its vibrational correction along axis τ. Within second-order vibrational perturbation theory (VPT2), ΔB_τ^{vib} is decomposed into harmonic (ΔB_τ^{harm}), Coriolis (ΔB_τ^{Cor}), and anharmonic (ΔB_τ^{anh}) contributions, the latter depending on semi-diagonal cubic force constants.[36] In this work, these terms are computed using a reduced-cost approach based on analytical gradients.[21,37] Vibrational corrections typically range from 0.3% to 0.7% of the rotational constant, and HPCS2 yields anharmonic corrections with errors below 10%,[38] making it suitable when 0.1% accuracy (i.e., spectroscopic accuracy) is targeted.

The characteristics of the different PCS variants[19] are summarized in Table 1.

Table 1: PCS variants used in this study. See main text for further details.

Label	**Valence (fc)**	**Core-valence (ae-fc)**	**Δ Valence (fc)**
HPCS2	B3LYP/6-31+G*	none	D3BJ
DPCS3	rev-DSD-PBEP86/3F12-	none	D3BJ
BDPCS3	rev-DSD-PBEP86/3F12-	CVB (Eq. 2)	D3BJ + VB (Eq. 3)

The energy thresholds adopted throughout the workflow are tailored to the system

and spectroscopic technique under study. A conservative detectability threshold is around 900 cm^{-1} (corresponding to ∼1% population at room temperature, where $kT/hc \approx 207$ cm^{-1}).[35,39,40] Standard energy cutoffs for successive steps are: 2500 cm^{-1} (initial sampling), 1500 cm^{-1} (intermediate refinement), and 1000 cm^{-1} (final selection). Additionally, relaxation to more stable conformers is considered probable when the associated barriers are below ∼400 cm^{-1}.[41–43] To account for such processes, HPCS2 relaxed scans were performed along soft degrees of freedom (notably exocyclic dihedrals), followed by TS optimization and characterization at the same level. Barrier heights were then refined via single-point DPCS3 energy calculations at HPCS2 geometries.

All calculations were performed using the Gaussian 16 package.[44] The BDPCS3 geometrical parameters were obtained from the corresponding DPCS3 bond lengths via the dedicated web platform available at `https://www.skiesvillage.it/proxima/pcsbonds/`.[45]

3 Results and Discussion

The conformational landscape of tiopronin is governed by several torsional degrees of freedom, as depicted in Figure 1. Dihedral angle labeling follows standard peptide nomenclature: for the i-th residue, ϕ_i = C'$_{i-1}$–N–C$^\alpha$–C'i, ψ_i = N–C$^\alpha$–C'–X, ω_i = C$^\alpha$–C'–X–Y, and χ_i^j denotes the j-th side-chain torsion. For the i-th non-terminal residue, X = N and Y = C$^\alpha i+1$, such that ω_1 remains close to 180°. On the other hand, for the terminal residue n (glycine in the case of tiopronin, with $n = 2$), X = O, Y = H, and ω_n can adopt either near-*cis* or near-*trans* configurations. Naturally, the ϕ_1 angle is undefined for tiopronin.

Dihedral angles are hereafter listed in the following order: ψ_1, ϕ_2, ψ_2, ω_2, and χ_1^1 (referred to simply as χ_1, since there is no ambiguity in the present case), with ω_1 not explicitly reported. Staggered conformations are denoted as g (60°), g^- (−60°), and a (180°), while s (0°), p (90°), ac^+ (120°), and ac^- (−120°) indicate syn, perpendicular, and anticlinal arrangements, respectively.

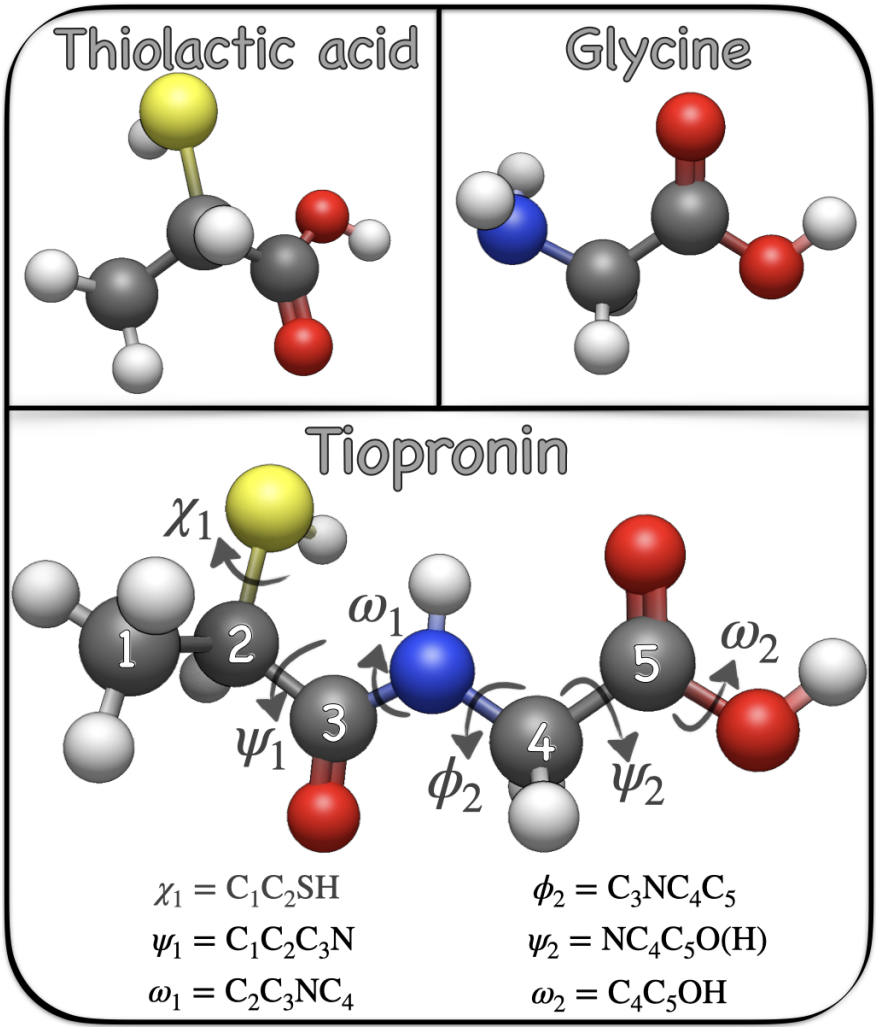

Figure 1: Structural motifs of thiolactic acid, glycine, and tiopronin. Atom numbering and dihedral angle labeling for tiopronin are also shown.

Low-energy conformers are stabilized by intramolecular hydrogen bonds that generate the pseudo-cyclic motifs defined in Table 2. Among these, C4 motifs form four-membered rings whose stabilization is governed by the planarity of the carboxylic group, itself favored by electron delocalization. The O–H···C=O interaction, although geometrically constrained, remains energetically favorable. C7 motifs generally provide greater stabilization than C5 ones, due to reduced ring strain. Thiol-based interactions (C5SH, C5S) are intrinsically weaker but may still contribute to the overall conformational stability when favorable spatial arrangements occur.[46–48]

C5 and C5OH rings necessarily coexist with C4 interactions due to shared geometric

constraints, while C7 and C4 motifs are mutually exclusive, as the formation of a C7 ring requires rotation of the ω_2 dihedral from trans to syn. C5S and C5SH motifs are generally compatible with other hydrogen bonds and can be further classified based on the χ_1 dihedral conformation (gauche or anti), as shown in Figure 2. These competing intramolecular interactions modulate the delicate balance between extended and folded geometries. Notably, extensive data on amino acids and peptide systems[7,26] support a consistent ranking of hydrogen-bond donor (O–H > N–H > S–H) and acceptor (N > C=O > OH > S) strengths. Accordingly, the O–H···C=O hydrogen bond in the C7 motif provides the strongest individual stabilization, followed by the analogous interactions in the C5 (highly bent) and C4 (highly strained) motifs. However, the combined stabilization from coexisting C5 and C4 interactions often exceeds that of a single C7 motif. Furthermore, the C5 motif is energetically more favorable than its C5OH analogue. Thiol-based hydrogen bonds, such as N–H···S (C5S) and S–H···N (C5SH), remain considerably weaker and only stabilize conformers when reinforced by stronger, concurrent interactions.

Table 2: Intramolecular hydrogen bonds in tiopronin. Atom labels follow Figure 1.

Cycle	**H-bond**	**Dihedrals**
C4	C5=O ··· HO	$\omega_2 = 180°$
C5	C5=O ··· HN	$\phi_2 = 180°$, $\psi_2 = 180°$, $\omega_2 = 180°$
C5OH	HO ··· HN	$\phi_2 = 180°$, $\psi_2 = 0°$, $\omega_2 = 180°$
C5SHg	SH ··· C3=O (gauche)	$\psi_1 = -120°$, $\chi_1 = -60°$
C5SHa	SH ··· C3=O (anti)	$\psi_1 = 0°$, $\chi_1 = 180°$
C5Sa	S ··· HN (anti)	$\psi_1 = 90°$, $\chi_1 = 180°$
C5Sg	S ··· HN (gauche)	$\psi_1 = 180°$, $120°$; $\chi_1 = \pm 60°$
C7	C3=O ··· HO	$\phi_2 = \pm 60°$, $\psi_2 = \mp 60°$, $\omega_2 = 0°$

A total of 25 distinct equilibrium conformers were identified (Table S1), 18 of which exhibit low interconversion barriers ($\Delta E_a < 400\text{cm}^{-1}$), suggesting rapid relaxation toward more stable structures under experimental conditions.[41,49] For each conformer, key geometrical parameters, dipole moments, relative electronic energies at the DPCS3 level (ΔE), zero-point vibrational corrections (ΔZPE), and thermodynamic contributions at 298.15K and 1atm are reported in the Supplementary Information (SI). A representative set of low-

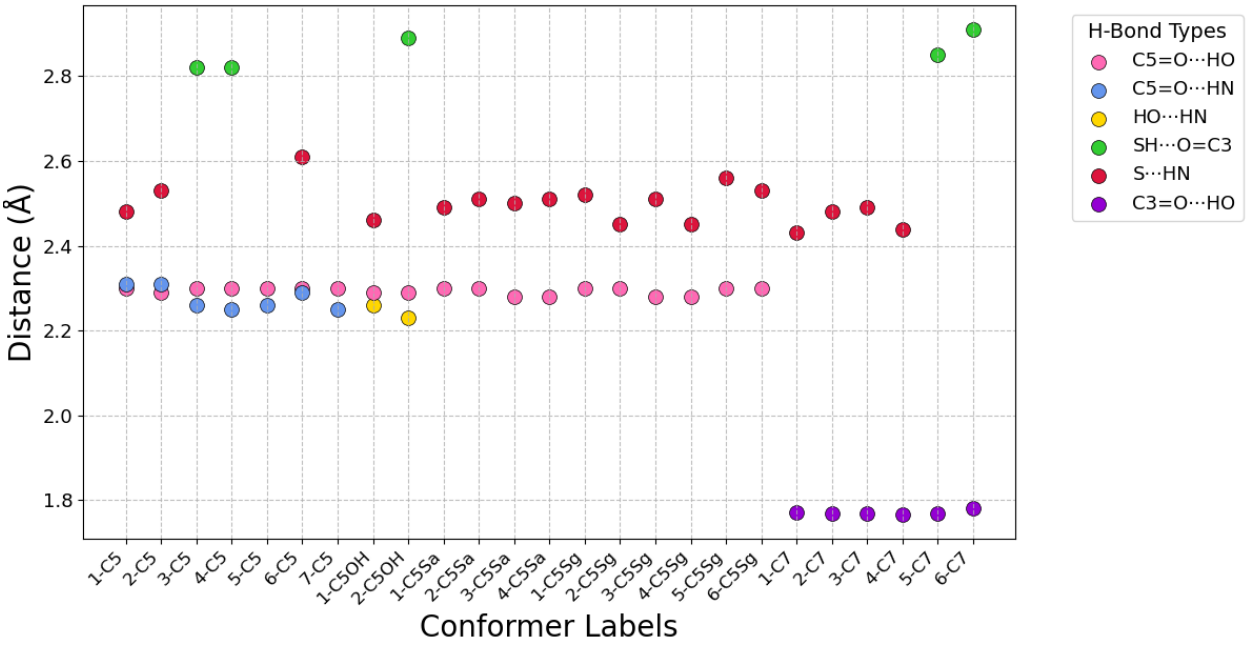

Figure 2: Hydrogen bond types which stabilize every conformer.

energy conformers, each associated with a distinct hydrogen-bond family, is summarized in Table3, with the corresponding structures illustrated in Figure 3.

The two most stable conformers, 1-C5 and 2-C5, are characterized by three hydrogen bonds forming C4, C5, and either C5Sg or C5Sa motifs. Additional C5-type structures (3-C5 through 7-C5), which feature C4 and C5 rings with secondary thiol-based interactions, relax readily to 1-C5 or 2-C5 via rotation around ψ_1 and/or χ_1, with barriers below 400 cm^{-1}.

Several low-lying conformers include C5S and C4 rings but lack the C5 interaction (e.g., 1–6-C5Sg, 1–4-C5Sa), and also relax efficiently toward more stable C5-type structures. Only one conformer, 1-C5OH, which features a C5OH pseudo-cycle, appears sufficiently kinetically stable to be potentially observable. It shows a population of ∼4% at 298.15K and relaxation barriers exceeding 500cm^{-1}. Its analogue, 2-C5OH, undergoes more facile relaxation to 3-C5.

In dipeptide analogues bearing terminal amide groups, the NH_2 fragment can form a C7 ring with the central carbonyl oxygen without compromising other stabilizing interactions.[7] In contrast, tiopronin's carboxylic terminus enforces formation of a C7 motif only at the expense of breaking the C4 hydrogen bond, due to the required ω_2 rotation from 180° to 0°.

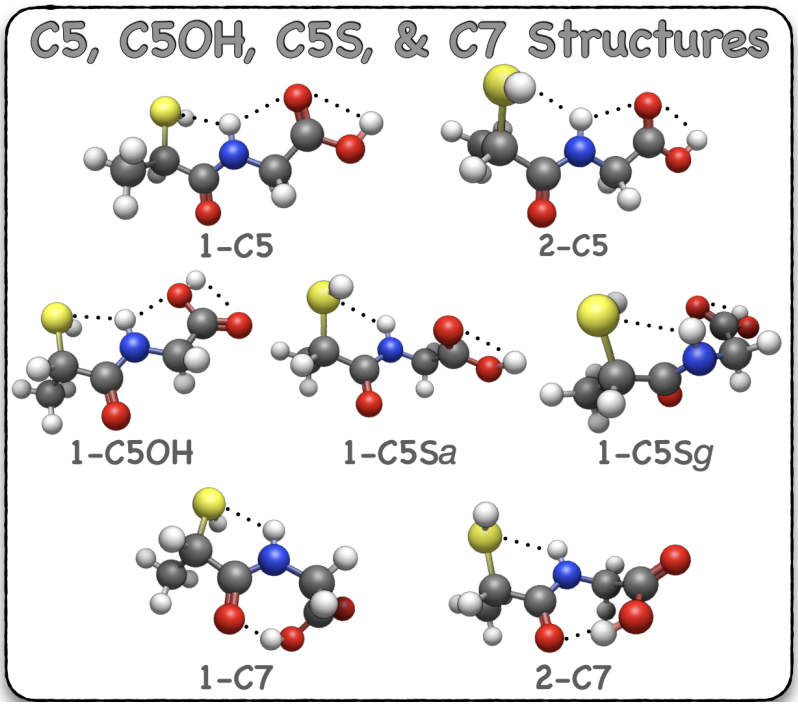

Figure 3: Lowest-energy conformers from different hydrogen-bonding classes.

As a result, the most stable C7 conformer lies roughly 330cm^{-1} above the global minimum (Table3), with entropic effects further destabilizing it. This makes its detection in the MW spectrum unlikely.

Table 3: Geometric parameters and relative DPCS3 electronic energies (ΔE), DPCS3 harmonic zero-point energies (ΔZPE), enthalpies [$\Delta(\Delta H)$], and entropies [$\Delta(T\Delta S)$] at 298.15 K and 1 atm of the different structures of tiopronin. All the values are in cm^{-1}. .

Conformers			ψ_1	ϕ_2	ψ_2	ω_2	χ_1	(ω_1)	ΔE[a]	ΔZPE[b]	$\Delta(\Delta H°)$[b,c]	$\Delta(T\Delta S°)$[b,d]	ΔE_a[e]
C5	1–C5	$\{ac^+,a,a,a,g^-\}$	132.9	178.1	-179.4	-179.7	-49.7	(178.2)	0.0	0.0	0.0	0.0	
	2–C5	$\{p,a,a,a,a\}$	99.4	-174.4	-179.4	-180.0	172.8	(-177.6)	-89.7	18.9	4.6	-70.5	$\{p,a,a,a,a\} \rightarrow \{ac^+,a,a,a,g^-\}$: 926.0
C5OH	1–C5OH	$\{ac^+,a,s,a,g^-\}$	133.5	166.5	5.2	178.9	-49.6	(178.0)	793.7	-20.4	26.3	1.2	$\{ac^+,a,s,a,g^-\} \rightarrow \{ac^+,a,a,a,g^-\}$: 564.8(564.7[f])
	2–C5OH	$\{ac^-,a,s,a,g^-\}$	-140.6	-175.5	-13.0	-178.3	-65.6	(-172.7)	877.3	-23.5	43.9	198.2	$\{ac^-,a,s,a,g^-\} \rightarrow \{ac^-,a,a,a,g^-\}$: 588.9(407.1[f])
C5S*a*	1–C5S*a*	$\{p,g^-,a,a,a\}$	89.3	-79.4	175.1	179.7	177.9	(170.7)	-84.1	117.0	-28.5	-124.0	$\{p,g^-,a,a,a\} \rightarrow \{p,a,a,a,a\}$: 178.4
	2–C5S*a*	$\{p,g^+,a,a,a\}$	100.8	77.7	-174.7	-179.7	174.9	(-165.1)	-0.7	94.2	-25.0	-158.9	$\{p,g^+,a,a,a\} \rightarrow \{p,a,a,a,a\}$: 149.9
C5S*g*	1–C5S*g*	$\{a,g^+,a,a,g^-\}$	171.9	72.7	-173.9	-179.6	-72.2	(-168.3)	-31.5	103.4	-45.2	-191.8	$\{a,g^+,a,a,g^-\} \rightarrow \{ac^+,a,a,a,g^-\}$: 238.2
	2–C5S*g*	$\{ac^+,g^-,a,a,g^-\}$	135.1	-77.2	173.8	179.6	-51.9	(168.8)	173.0	77.5	-29.8	-68.5	$\{ac^+,g^-,a,a,g^-\} \rightarrow \{ac^+,a,a,a,g^-\}$: 11.30
C7	1–C7	$\{ac^+,g^+,g^-,s,g^-\}$	135.9	76.8	-59.6	0.3	-47.7	(173.1)	90.4	268.9	-133.2	-521.3	
	2–C7	$\{p,g^-,g^+,s,a\}$	100.3	-76.4	59.4	-0.4	170.0	(-171.9)	9.5	284.0	-125.3	-583.1	

[a] DPCS3 electronic energies. [b] DPCS3 harmonic values. [c] Difference between the enthalpy at 298.15 K and 0 K. [d] At 298.15 K. [e] Single point DPCS3 at HPCS2 geometries, including harmonic HPCS2 ZPE corrections. [f] DPCS3 electronic energy including harmonic HPCS2 ZPE corrections.

In summary, assuming full conformational relaxation during supersonic expansion, the 1-C5 and 2-C5 species are expected to dominate the experimental spectrum. These conformers combine high stability with substantial dipole moments (ca. 1.7 D, predominantly along

the a axis), high Boltzmann populations, and interconversion barriers close to 1000cm^{-1} (Table3). The 1-C5OH conformer may also be observable, given its sizable dipole moment (ca. 3.0 D, dominant b component), non-negligible population (4%), and relaxation barriers exceeding 500cm^{-1}. In contrast, C7-type conformers, despite their large dipole moments (above 5 D, with strong a-axis contributions), are likely spectroscopically silent due to their low populations and rapid relaxation pathways.

Figures 4 and S1 compare the experimental spectrum (black lines) with the theoretical predictions for the 1–C5 and 2–C5 conformers of tiopronin, computed at various levels of theory. Based on previous benchmarks,[28] the BDPCS3//HPCS2 model was selected as a reliable starting point for spectral assignment, as it yields vibrationally averaged rotational constants with near-spectroscopic accuracy. The corresponding transitions are reported in panel (d) of both figures.

The two most populated conformers exhibit dominant μ_a dipole moment components, with smaller contributions from μ_b and μ_c (see Table 5). The assignment of the experimental spectrum began with the lowest-energy conformer, 1–C5, corresponding to the $\{ac^+, a, a, a, g^-\}$ dihedral arrangement. The strongest $^aR_{0,1}$ transitions ($\Delta J = +1$, $\Delta K_a = 0$, $\Delta K_c = 1$ with $K_c = 1$) were identified first using the JB95 software.[50] The observed lines were fitted using the SPFIT program[51–54] within the Watson A-reduced Hamiltonian for a prolate asymmetric top, which is appropriate given the nearly prolate nature of tiopronin conformers ($\kappa \approx -1$).[55] Subsequent ^bR and ^cR transitions were then identified.

For 1–C5, a total of 165 transitions were assigned and fitted with a root-mean-square deviation (σ) of 30 kHz. The same protocol was applied to the second most stable conformer, 2–C5 ($\{p, a, a, a, a\}$), for which 111 lines were assigned with a fitting accuracy of $\sigma \approx 33$ kHz. In both cases, the nuclear quadrupole coupling due to the ^{14}N nucleus ($I = 1$) was also resolved. This interaction splits each rotational level into three F sublevels, with $F = |J - I|, \ldots, J + I$.[56] Figure 5 shows the hyperfine structure of selected transitions: the $4_{2,3} \leftarrow 3_{1,2}$ line of 1–C5 exhibits three resolved components ($F = 3 \leftarrow 2$, $F = 5 \leftarrow 4$,

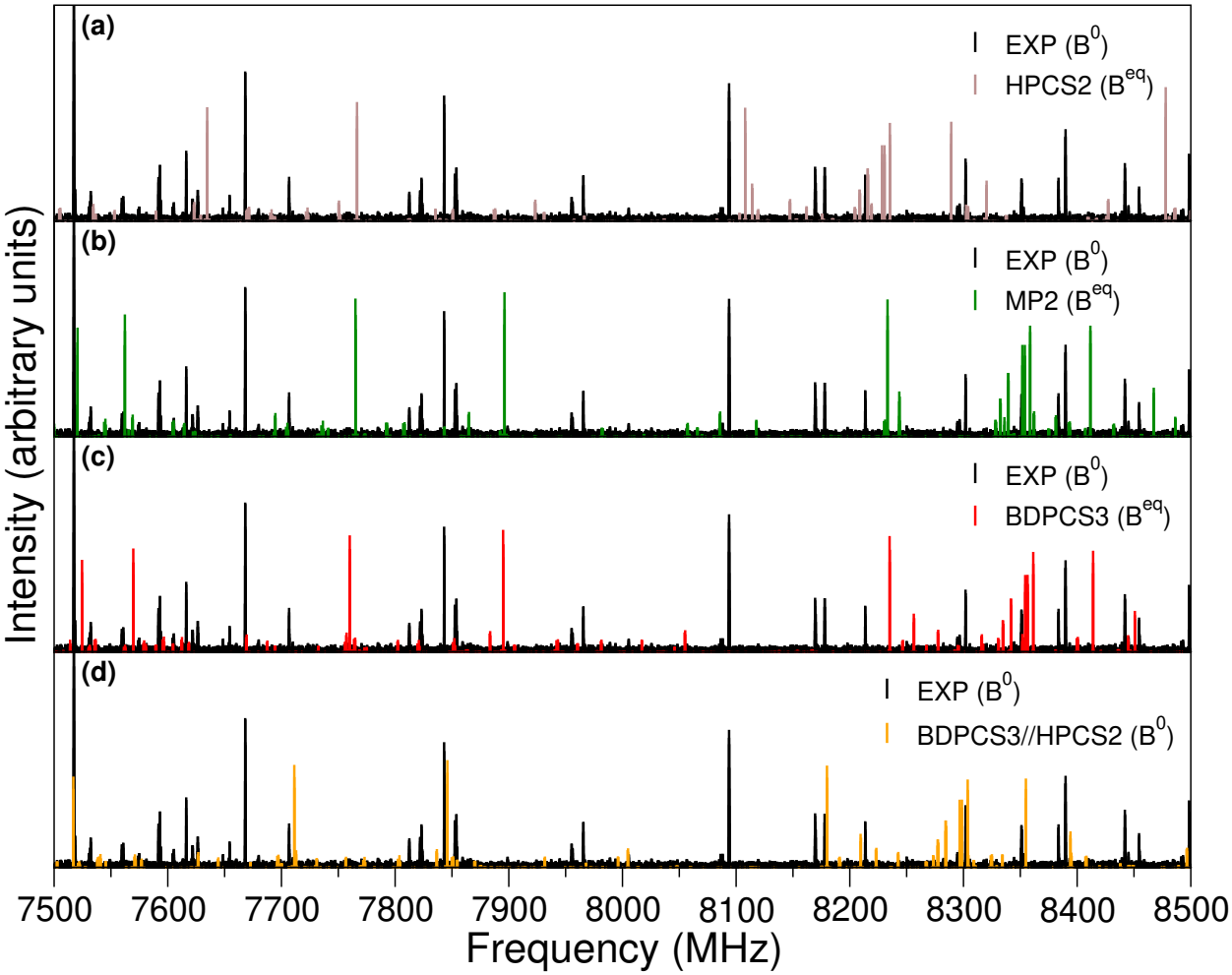

Figure 4: The experimental spectrum (black lines) is compared with theoretical spectra derived from different levels of theory for the 1–C5 conformer. Panels (a), (b), and (c) display the theoretical spectra calculated using the HPCS2, MP2, and BDPCS3 methodologies, respectively. Panel (d) shows the transition positions obtained by incorporating HPCS2 vibrational corrections into the BDPCS3 model. The spectral results for the 2-C5 conformer are presented in Figure S1.

$F = 4 \leftarrow 3$), while the $3_{2,1} \leftarrow 2_{1,2}$ transition of 2–C5 splits into $F = 3 \leftarrow 2$, $F = 4 \leftarrow 3$, and $F = 2 \leftarrow 1$ components. All measured transitions are listed in Tables S4 and S5.

Figure 5 displays the fitted transitions for both identified conformers. Notably, the most intense features—belonging to the ${}^{a}R$ branch—were accurately reproduced only when vibrational corrections were incorporated into the BDPCS3 model. This demonstrates that such corrections are essential for reliable spectral assignment in congested regions, particularly for flexible molecules (see panel (d) in Figures 4 and S1, and compare with the labeled ${}^{a}R_{0,1}$

Table 4: Experimental spectroscopic constants (A_0, B_0, C_0, χ_{aa}, χ_{bb}, and χ_{cc} in MHz) of the 1–C5 and 2–C5 conformers in Watson's A-reduced prolate asymmetric rotor Hamiltonian.

	1–C5 $\{ac^+, a, a, a, g^-\}$	2–C5 $\{p, a, a, a, a\}$
A_0	2036.04196(90)	1943.32499(125)
B_0	571.61479(50)	578.71821(80)
C_0	459.93631(60)	478.12871(74)
χ_{aa}	2.527(1)	2.531(2)
χ_{bb}	1.2768(54)	-1.1186(17)
χ_{cc}	-3.8041(54)	-3.6499(17)
$N^{[a]}$	165	111
$\sigma^{[b]}$	29.45	33.44

[a] Number of measured transitions. [b] RMS deviation of the fit (in kHz).

transitions in Figure 5).

Despite our thorough search, several spectral lines remained unaccounted for that did not belong to the 1-C5 and 2-C5 conformers. Initially, we considered the possibility that these lines might be due to the 1-C5OH conformer, which we estimated to have approximately 4% population. However, no spectral match was possible for this conformer. This absence can be explained by examining the overall signal intensity in our experiment: the signals of the already detected conformers were relatively weak due to the challenging nature of the laser ablation experiment and the complex hyperfine structure that spreads the signal intensity across multiple components. As can be inferred from the rotational spectrum in Figure 5, any signals from this minor species would fall below the signal-to-noise ratio.

We then explored alternative explanations for the unassigned spectral lines. One possibility we investigated was that these transitions might result from the splitting of rotational lines into doublets due to internal rotation of the methyl group, a phenomenon well-documented in microwave spectroscopy.[56] To investigate this possibility systematically, we performed a relaxed Potential Energy Surface (PES) scan of the methyl group rotation (see Figure SX). Our calculations revealed a substantial torsional barrier height of approximately 1250

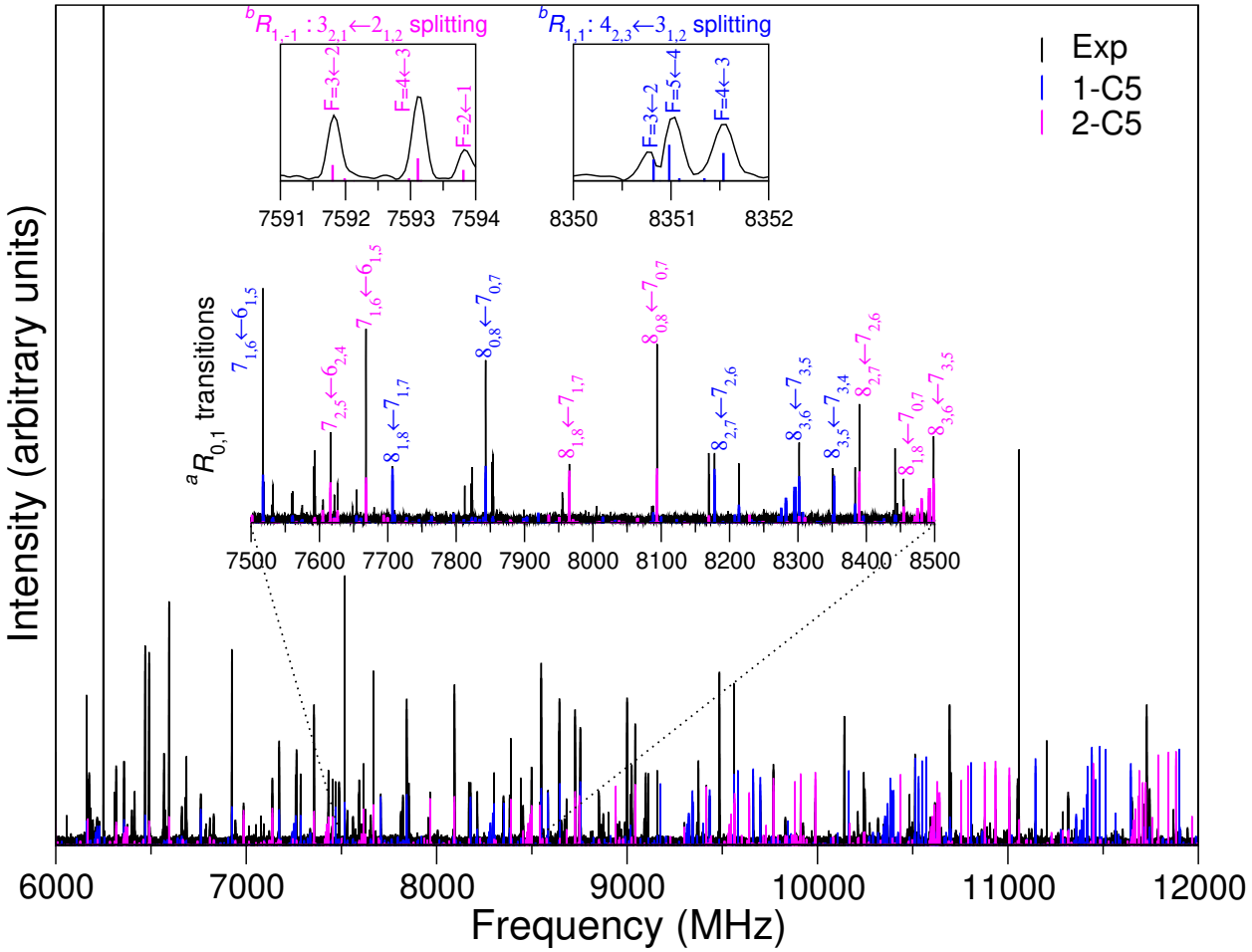

Figure 5: Broadband rotational spectrum of tiopronin in the 6–12 GHz frequency region using the LA-CP-FTMW spectrometer. The fitted spectral lines corresponding to the two identified conformers are highlighted. The blue lines correspond to some $^{a}R_{0,1}$ transitions detected within the $7.5 - 8.5$ GHz range are labeled. Quadrupole hyperfine splittings are shown for: (i) the $3_{2,1} \leftarrow 2_{1,2}$ of the 2–C5 conformer, (ii) the $4_{2,3} \leftarrow 3_{1,2}$ transitions of the 1–C5 conformer.

cm^{-1} for both detected conformers. This high barrier effectively prevents observable methyl rotation at our experimental temperatures, confirming that A-E splitting should not be detectable in the spectrum and thus eliminating this as a potential source of the unassigned lines.

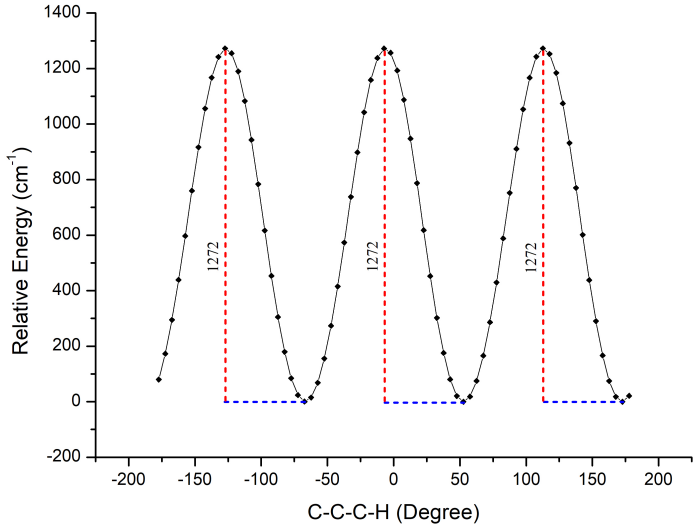

Figure 6: Potential energy curve governing methyl rotation.

Having ruled out both the minor conformer and methyl rotation effects, we subsequently turned our attention to possible molecular fragments generated during the laser ablation process. This approach was informed by our previous work,[57] where we demonstrated that laser ablation of nonvolatile solid organic precursors can produce a rich variety of smaller molecular species. The high-energy laser pulse can break various bonds in the parent molecule, creating reactive fragments that may recombine or stabilize as smaller molecules.

Our analysis revealed that the laser ablation of tiopronin, despite being a relatively simple molecule, generates a remarkable diversity of molecular fragments. We identified several nitrogen-containing species including isothiocyanic acid (HNCS), cyanoacetylene (HC_3N), ethyl cyanide (C_2H_5CN), vinyl cyanide (C_2H_3CN), methylcyanoacetylene (CH_3C_3N), vinyl cyanoacetylene (C_4H_3N), cyanodiacetylene (HC_5N), and cyanoallene ($H_2CCCHCN$). These nitrogenous fragments likely originate from the cleavage of the amide bond in tiopronin,

followed by various recombination processes.

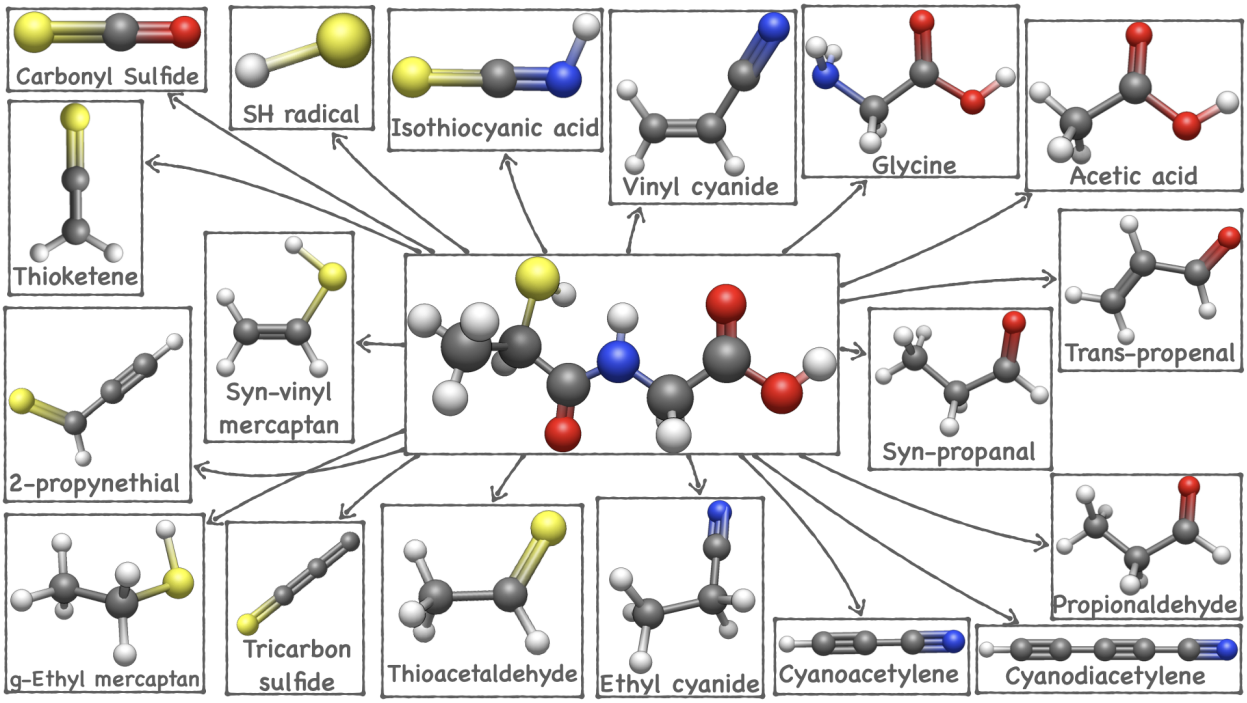

Figure 7: Fragments detected in the rotational spectra of laser-ablated tiopronin.

Additionally, we detected several sulfur-containing species such as thioacetaldehyde (CH_3CHS), thioketene ($H_2C{=}C{=}S$), syn-vinyl mercaptan ($CH_2{=}CHSH$), carbonyl sulfide (OCS), propynethial ($HC_2CH{=}S$), tricarbon monosulfide (C_3S), gauche-ethyl mercaptan (C_2H_5SH), and thioformamide ($HC(S)NH_2$). The presence of these sulfur-containing fragments is particularly noteworthy given tiopronin's terminal thiol group, which appears to participate in diverse fragmentation and recombination pathways. We also identified trans-propenal ($CH_2{=}CH\text{-}CHO$) among the fragments, which likely forms through oxygen-containing moiety rearrangements.

The identification of these fragments not only helps explain some of the unassigned spectral features but also provides valuable insights into the chemical behavior of tiopronin under high-energy conditions. The fragmentation pattern reveals preferential bond cleavage sites and subsequent reaction pathways that may be relevant to understanding the molecular stability and reactivity of thiolated peptide analogues in various environments. Furthermore,

several of these fragments, particularly the simple nitriles and sulfur-containing species, have been detected in interstellar media and are considered potentially important in prebiotic chemical evolution scenarios. Their formation from tiopronin under our experimental conditions may thus have implications for understanding possible degradation and transformation pathways of similar molecules in prebiotic contexts.

In Table 5 the computed rotational constants of 1–C5 and 2–C5 conformers are compared with the experimental values for the two conformers unambiguously identified in the MW spectrum. The corresponding absolute (MAX and MUE) and relative (%MAX and %MUE) errors highlight the following trends: (i) HPCS2 and MP2//HPCS2 rotational constants systematically underestimate the experimental values by approximately 2% and 1%, respectively; (ii) DPCS3//HPCS2 predictions reduce the average error to around 0.5%; and (iii) BDPCS3//HPCS2 further improves the agreement, yielding the most accurate results.

These findings confirm that BDPCS3//HPCS2 provides ground-state rotational constants of sufficient accuracy to guide experimental spectral assignments. Remarkably, the deviations obtained with this model are comparable to those achieved for the glycine dipeptide analogue using a significantly more expensive composite quantum-chemical approach (MUE%=0.3, MAX%=0.6).[7]

Table 5: Experimental and computed ground state rotational constants (A_0, B_0, C_0 in MHz), together with HPCS2 vibrational corrections (ΔB_τ^{vib} in MHz) of the observed structures. Absolute mean and maximum unsigned errors between computed and experimental rotational constants (MUE and MAX in MHz) and the corresponding relative values (MUE% and MAX%) are also reported.

Conformer	**Parameter**	**Exp**	**HPCS2**	**MP2**	**DPCS3**	**BDPCS3**	**ΔVib**
1–C5 $\{ac^+, a, a, a, g^-\}$	A_0	2036.0	1984.5	1982.0	2010.1	2019.5	11.6
	B_0	571.6	563.3	570.5	569.7	571.4	4.3
	C_0	459.9	452.7	461.1	458.8	460.4	2.8
	MUE		22.4	18.8	9.6	5.7	
	MAX		51.6	54.1	25.9	16.5	
	MUE%		1.9	1.0	0.6	0.3	
	MAX%		2.5	2.7	1.3	0.8	
	χ_{aa}	2.527	2.578	2.578	2.527	—	—
	χ_{bb}	1.277	1.399	1.390	1.320	—	—

Continuation of Table 5.

Conformer	Parameter	Exp	HPCS2	MP2	DPCS3	BDPCS3	ΔB_{τ}^{vib}
	χ_{cc}	-3.804	-3.978	-3.968	-3.847	—	—
2–C5 $\{p, a, a, a, a\}$	A_0	1943.3	1889.3	1898.2	1924.2	1933.2	9.1
	B_0	578.7	568.5	575.9	575.9	577.7	4.5
	C_0	478.1	472.9	484.2	477.3	478.9	3.4
	MUE		23.1	18.0	7.6	3.9	
	MAX		54.0	45.1	19.1	10.1	
	MUE%		1.9	1.4	0.5	0.3	
	MAX%		2.8	2.3	1.0	0.5	
	χ_{aa}	2.531	2.605	2.655	2.555	—	—
	χ_{bb}	1.119	1.211	1.139	1.137	—	—
	χ_{cc}	-3.650	-3.816	-3.794	-3.692	—	—
1–C5OH $\{ac^+, a, s, a, g^-\}$	A_0	—	1955.6	1910.9	1958.4	1967.4	16.9
	B_0	—	559.3	568.7	567.9	569.7	3.7
	C_0	—	442.7	456.4	452.9	454.4	1.9
	χ_{aa}	—	2.567	2.604	2.576	—	—
	χ_{bb}	—	1.437	1.395	1.381	—	—
	χ_{cc}	—	-4.004	-3.998	-3.958	—	—
1–C7 $\{p, g^-, g^+, s, a\}$	A_0	—	2153.9	2167.5	2188.0	2197.9	11.6
	B_0	—	577.6	585.5	585.6	587.2	4.7
	C_0	—	516.0	524.4	521.7	523.2	4.3
	χ_{aa}	—	1.933	2.065	1.674	—	—
	χ_{bb}	—	1.436	1.328	0.679	—	—
	χ_{cc}	—	-3.369	-3.393	2.353	—	—
2–C7 $\{ac^+, g^+, g^-, s, g^-\}$	A_0	—	2060.6	2066.1	2082.7	2092.0	16.6
	B_0	—	595.5	604.9	604.0	605.8	3.5
	C_0	—	517.0	525.2	525.4	527.0	3.2
	χ_{aa}	—	1.608	1.689	2.023	—	—
	χ_{bb}	—	0.720	0.517	1.250	—	—
	χ_{cc}	—	-2.328	-2.006	-3.272	—	—

Overall, the excellent agreement between computed and experimental spectra confirms the robustness of the BDPCS3//HPCS2 protocol and supports its application to the accurate structural characterization of flexible, biologically, and prebiotically relevant molecules.

4 Conclusions

In this work, we have investigated the conformational landscape of tiopronin, a thiol-terminated N-substituted amino acid of prebiotic relevance, by combining high-resolution rotational spectroscopy with accurate quantum-chemical calculations. Using an unsupervised computational tool that integrates several methods and couples high accuracy with reasonable computational cost, we predicted equilibrium and vibrationally corrected rotational constants for several low-energy conformers. These theoretical results enabled direct comparison with experimental data and allowed for the unambiguous identification of the most populated structures under jet-cooled conditions.

Our findings underscore the value of synergistic strategies that integrate spectroscopic techniques with advanced computational models to unravel the structural complexity of flexible biomolecules. In particular, the successful characterization of tiopronin demonstrates that sulfur-containing peptide analogues can be studied with high accuracy, offering structural insight into chemical motifs of potential relevance to prebiotic evolution.

Beyond the specific case of tiopronin, the methodology and results presented here define a robust framework for the investigation of analogous systems. This approach opens the way to future studies on prebiotic peptide candidates and other biologically inspired, flexible molecules.

Conflict of Interest Disclosure

The authors declare no competing financial interest.

Acknowledgement

Funding from Gaussian Inc. is gratefully acknowledged by the Italian authors.

Supporting Information Available

Additional computational and experimental details. Dihedral angles, relative stabilities, dipole moments, relative populations and DPCS3 equilibrium geometries of all low-energy conformers. Measured rotational transitions of the detected conformers. This material is available free of charge via the Internet.

References

(1) Clayden, J.; Greeves, N.; Warren, S. *Organic Chemistry*; OUP Oxford, 2012.

(2) Frenkel-Pinter, M.; Samanta, M.; Ashkenasy, G.; Leman, L. J. Prebiotic peptides: Molecular hubs in the origin of life. *Chem. Rev.* **2020**, *120*, 4707–4765.

(3) Frenkel-Pinter, M.; Bouza, M.; Fernández, F. M.; Leman, L. J.; Williams, L. D.; Hud, N. V.; Guzman-Martinez, A. Thioesters provide a plausible prebiotic path to proto-peptides. *Nature Communications* **2022**, *13*, 2569.

(4) Lesarri, A.; Mata, S.; López, J. C.; Alonso, J. L. A Laser-Ablation Molecular-Beam Fourier-Transform Microwave Spectrometer: The Rotational Spectrum of Organic Solids. *Rev. Scient. Instrum.* **2003**, *74*, 4799–4804.

(5) Blanco, S.; Lesarri, A.; López, J. C.; Alonso, J. L. The Gas-Phase Structure of Alanine. *J. Am. Chem. Soc.* **2004**, *126*, 11675–11683.

(6) Sanz, M. E.; Blanco, S.; López, J. C.; Alonso, J. L. Rotational Probes of Six Conformers of Neutral Cysteine. *Angew. Chem. Int. Ed.* **2008**, *47*, 6216–6220.

(7) Puzzarini, C.; Biczysko, M.; Barone, V.; Largo, L.; Peña, I.; Cabezas, C.; Alonso, J. L. Accurate characterization of the peptide linkage in the gas phase: A joint quantum-chemical and rotational spectroscopy study of the glycine dipeptide analogue. *J. Phys. Chem. Lett.* **2014**, *5*, 534–540.

(8) Alonso, J. L.; López, J. C. *Gas-Phase IR Spectroscopy and Structure of Biological Molecules*; Springer, 2015; pp 335–401.

(9) León, I.; Alonso, E. R.; Mata, S.; Cabezas, C.; Alonso, J. L. Unveiling the Neutral Forms of Glutamine. *Angew. Chem. Int. Ed.* **2019**, *58*, 16002–16007.

(10) Brown, G. G.; Dian, B. C.; Douglass, K. O.; Geyer, S. M.; Shipman, S. T.; Pate, B. H. A Broadband Fourier Transform Microwave Spectrometer Based on Chirped Pulse Excitation. *Rev. Sci. Instrum.* **2008**, *79*, 053103.

(11) Steber, A. L.; Neill, J. L.; Zaleski, D. P.; Pate, B. H.; Lesarri, A.; Bird, R. G.; Vaquero-Vara, V.; Pratt, D. W. Structural Studies of Biomolecules in the Gas Phase by Chirped-Pulse Fourier Transform Microwave Spectroscopy. *Faraday Discuss.* **2011**, *150*, 227–242.

(12) Pérez, C.; Neill, J. L.; Muckle, M. T.; Zaleski, D. P.; Peña, I.; López, J. C.; Alonso, J. L.; Pate, B. H. Water–Water and Water–Solute Interactions in Microsolvated Organic Complexes. *Angew. Chem. Int. Ed.* **2015**, *54*, 979–982.

(13) Steber, A. L.; Pérez, C.; Temelso, B.; Shields, G. C.; Rijs, A. M.; Pate, B. H.; Kisiel, Z.; Schnell, M. Capturing the Elusive Water Trimer from the Stepwise Growth of Water on the Surface of the Polycyclic Aromatic Hydrocarbon Acenaphthene. *J. Phys. Chem. Lett.* **2017**, *8*, 5744–5750.

(14) Puzzarini, C.; Spada, L.; Alessandrini, S.; Barone, V. The Challenge of Non-Covalent Interactions: Theory Meets Experiment for Reconciling Accuracy and Interpretation. *J. Phys.: Condens. Matter* **2020**, *32*, 343002.

(15) Xie, F.; Fusè, M.; Hazrah, S., A.; Jaeger, W.; Barone, V.; Xu, Y. Discovering the Elusive Global Minimum in a Ternary Chiral Cluster: Rotational Spectra of Propylene Oxide Trimer. *Angew. Chem. Int. Ed.* **2020**, *59*, 22427–22430.

(16) Cabezas, C.; Varela, M.; Alonso, J. L. The Structure of the Elusive Simplest Dipeptide Gly-Gly. *Angew. Chem.* **2017**, *129*, 6520–6525.

(17) León, I.; Alonso, E. R.; Mata, S.; Alonso, J. L. A rotational study of the AlaAla dipeptide. *Phys. Chem. Chem. Phys.* **2020**, *22*, 13867–13871.

(18) Sahoo, N. P.; Franke, P. R.; Stanton, J. F. On the Performance of composite Schemes in Determining Equilibrium Molecular Structures. *J. comput. Chem.* **2024**, *45*, 1419–1427.

(19) Di Grande, S.; Barone, V. Toward Accurate Quantum Chemical Methods for Molecules of Increasing Dimension: the New Family of Pisa Composite Schemes. *J. Phys. Chem. A* **2024**, *128*, 4886–4900.

(20) Barone, V. From perception to prediction and interpretation: enlightening the gray zone of molecular bricks of life with the help of machine learning and quantum chemistry. *WIREs Comput. Mol. Sci.* **2025**, *15*, e:70000.

(21) Mendolicchio, M.; Barone, V. Accurate Vibrational and Ro-vibrational Contributions to the Properties of Large Molecules by a New Engine Employing Curvilinear Internal Coordinates and Vibrational Perturbation Theory to Second Order. *J. Chem. Theory Comput.* **2024**, *20*, 8378–8395.

(22) Mato, S.; Pe˜na, I.; Cabezas, C.; L´opez, J. C.; Alonso, J. A Broadband Fourier Transform Microwave Spectrometer With Laser Ablation Source: The Rotational Spectrum of Nicotinic Acid. *J. Mol. Spectrosc.* **2012**, *280*, 91–96.

(23) Mato, S.; Aguado, R.; Mata, S.; Alonso, J. L.; León, I. *Phys. Chem. Chem. Phys.* **2022**, *24*, 24032–24038.

(24) Aguado, R.; Mata, S.; Sanz-Novo, M.; Alonso, E. R.; León, I.; Alonso, J. L. *J. Phys. Chem. Lett.* **2022**, *13*, 9991–9996.

(25) Mancini, G.; Fusè, M.; Lazzari, F.; Barone, V. Fast Exploration of Potential Energy Surfaces With a Joint Venture of Quantum Chemistry, Evolutionary Algorithms and Unsupervised Learning. *Digital Discovery* **2022**, *1*, 10539–10547.

(26) Barone, V.; Fusè, M.; Lazzari, F.; Mancini, G. Benchmark Structures and Conformational Landscapes of Amino Acids in the Gas Phase: a Joint Venture of Machine

Learning, Quantum Chemistry, and Rotational Spectroscopy. *J. Chem. Theory Comput.* **2023**, *19*, 1243–1260.

(27) Barone, V. et al. Bringing Machine-Learning Enhanced Quantum Chemistry and Microwave Spectroscopy to Conformational Landscape Exploration: the Paradigmatic Case of 4-Fluoro-Threonine. *Chemistry, Europ. J.* **2023**, e202203990.

(28) Lazzari, F.; Uribe, L.; Di Grande, S.; Crisci, L.; Mendolicchio, M.; Barone, V. Structures and Rotational Constants of Monocyclic Monoterpenes at DFT Cost by Pisa Composite Schemes and Vibrational Perturbation Theory. *J. Phys. Chem. A* **2024**, *128*, in press.

(29) MacroModel, S. Schrödinger Release 2025-2. **LLC, New York, NY, 2025**,

(30) Santra, G.; Sylvetsky, N.; Martin, J. M. Minimally Empirical Double-Hybrid Functionals Trained Against the GMTKN55 Database: revDSD-PBEP86-D4, revDOD-PBE-D4, and DOD-SCAN-D4. *J. Phys. Chem. A* **2019**, *123*, 5129–5143.

(31) Barone, V. Accuracy Meets Feasibility for the Structures and Rotational Constants of the Molecular Bricks of Life: a Joint Venture of DFT and Wave-Function Methods. *J. Phys. Chem. Lett.* **2023**, *14*, 5883–5890.

(32) Peterson, K. A.; Adler, T. B.; Werner, H.-J. Systematically Convergent Basis Sets for Explicitly Correlated Wavefunctions: The Atoms H, He, B–Ne, and Al–Ar. *J. Chem. Phys.* **2008**, *128*, 084102.

(33) Dunning, T. H. Gaussian Basis Sets for Use in Correlated Molecular Calculations. I. The Atoms Boron Through Neon and Hydrogen. *J. Chem. Phys.* **1989**, *90*, 1007–1023.

(34) Barone, V. PCS/Bonds: Pick your Molecule and Get Its Accurate Structure and Rotational Constants at DFT Cost. *J. Chem. Phys.* **2023**, *159*, 081102.

(35) Barone, V. Quantum Chemistry Meets High-Resolution Spectroscopy for Characterizing the Molecular Bricks of Life in the Gas-Phase. *Phys. Chem. Chem. Phys.* **2024**, *26*, 5802–5821.

(36) Puzzarini, C.; Stanton, J. F.; Gauss, J. Quantum-Chemical Calculation of Spectroscopic Parameters for Rotational Spectroscopy. *Int. Rev. Phys. Chem.* **2010**, *29*, 273–367.

(37) Mendolicchio, M.; Barone, V. Unbiased Comparison Between Theoretical and Experimental Molecular Structures and Properties: Toward an Accurate Reduced-Cost Evaluation of Vibrational Contributions. *J. Chem. Theory Comput.* **2024**, *20*, 2842–2857.

(38) Piccardo, M.; Penocchio, E.; Puzzarini, C.; Biczysko, M.; Barone, V. Semi-experimental equilibrium structure determinations by employing B3LYP/SNSD anharmonic force fields: Validation and application to semirigid organic molecules. *J. Phys. Chem. A* **2015**, *119*, 2058–2082.

(39) Alonso, E. R.; León, I.; Alonso, J. L. *Intra- and Intermolecular Interactions Between Non-Covalently Bonded Species*; Elsevier, 2020; pp 93–141.

(40) León, I.; Fusè, M.; Alonso, E. R.; Mata, S.; Mancini, G.; Puzzarini, C.; Alonso, E. R.; Barone, V. Unbiased Disentanglement of Conformational Baths With the Help of Microwave Spectroscopy, Quantum Chemistry and Artificial Intelligence: the Puzzling Case of Homocysteine. *J. Chem. Phys.* **2022**, *157*, 074107.

(41) Ruoff, R. S.; Klots, T. D.; Emilsson, T.; Gutowsky, H. S. Relaxation of Conformers and Isomers in Seeded Supersonic Jets of Inert Gases. *J. Chem. Phys.* **1990**, *93*, 3142–3150.

(42) Godfrey, P. D.; Brown, R. D. Proportions of Species Observed in Jet Spectroscopy-Vibrational Energy Effects: Histamine Tautomers and Conformers. *J. Am. Chem. Soc.* **1998**, *120*, 10724–10732.

(43) Florio, G. M.; Christie, R. A.; Jordan, K. D.; Zwier, T. S. Conformational Preferences of Jet-Cooled Melatonin: Probing Trans- and Cis-Amide Regions of the Potential Energy Surface. *J. Am. Chem. Soc.* **2002**, *124*, 10236–10247.

(44) Frisch, M. J.; Trucks, G. W.; Schlegel, H. B.; Scuseria, G. E.; Robb, M. A.; Cheeseman, J. R.; Scalmani, G.; Barone, V.; Petersson, G. A.; Nakatsuji, H.; others Gaussian 16 Revision C.01. Gaussian Inc. Wallingford CT 2016.

(45) Barone, V.; Lazzari, F. Hunting For Complex Organic Molecules In The Interstellar Medium: The Role Of Accurate Low-Cost Theoretical Geometries And Rotational Constants. *J. Phys. Chem. A* **2023**, *127*, 10517–10527.

(46) Weinhold, F.; Landis, C. R. *Valency and Bonding: A Natural Bond Orbital Donor-Acceptor Perspective*; Cambridge University Press, 2005.

(47) Gilli, G.; Gilli, P. *The Nature of the Hydrogen Bond: Outline of a Comprehensive Hydrogen Bond Theory*; Oxford University Press, 2009.

(48) Colizzi, F.; Bussi, G. On the Relative Stability of Cis and Trans Proline Conformers in Water: Free Energy and Kinetics. *The Journal of Physical Chemistry B* **2019**, *123*, 5894–5903.

(49) Godfrey, P. D.; Brown, R. D.; Rodgers, F. M. The Missing Conformers of Glycine and Alanine: Relaxation in Seeded Supersonic Jets. *J. Mol. Struct.* **1996**, *376*, 65–81.

(50) Plusquellic, D. F. JB95 Spectral fitting program. (accessed: 26.04.2025); `NISThttps://www.nist.gov/services-resources/software/jb95-spectral-fitting-program`.

(51) Pickett, H. M. The Fitting and Prediction of Vibration-Rotation Spectra with Spin Interactions. *J. Mol. Spectrosc.* **1991**, *148*, 371–377.

(52) Kisiel, Z.; Pszczółkowski, L.; Medvedev, I. R.; Winnewisser, M.; De Lucia, F. C.;

Herbst, E. Rotational Spectrum of Trans-Trans Diethyl Ether in the Ground and Three Excited Vibrational States. *J. Mol. Spectrosc.* **2005**, *233*, 231–243.

(53) Kisiel, Z. Software Packages for Broadband High-Resolution Spectroscopy. (accessed: 26.04.2025); `http://info.ifpan.edu.pl/~kisiel/prospe.htm#use`.

(54) Kisiel, Z. PROSPE - Programs for ROtational SPEctroscopy. (accessed: 26.04.2025); `https://www.ifpan.edu.pl/~kisiel/prospe.htm`.

(55) Ray, B. S. Über die Eigenwerte des asymmetrischen Kreisels. *Zeitschr. Phys.* **1932**, *78*, 74–91.

(56) Gordy, W.; Cook, R. L. *Microwave molecular spectra*; Interscience Pub., 1984.

(57) Kolesniková, L.; León, I.; Alonso, E. R.; Mata, S.; alonso, j. L. An Innovative Approach for the Generation of Species of the Interstellar Medium. *Angew. Chem. Int. Ed. Engl.* **2021**, *133*, 24666–24671.

TOC Graphic

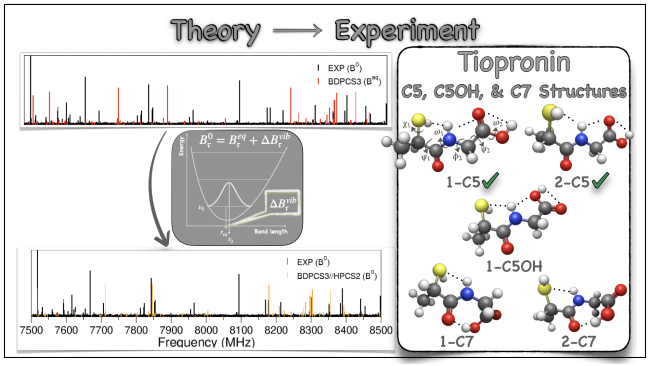
Theory ⟶ Experiment
EXP (B^0)
BDPCS3 (B^{eq})
$B_\tau^0 = B_\tau^{eq} + \Delta B_\tau^{vib}$
ΔB_τ^{vib}
Bond length
EXP (B^0)
BDPCS3//HPCS2 (B^0)
7500 7600 7700 7800 7900 8000 8100 8200 8300 8400 8500
Frequency (MHz)
Tiopronin
C5, C5OH, & C7 Structures
1-C5
2-C5
1-C5OH
1-C7
2-C7